

# Evidence for a Supershear Transient during the 2002 Denali Fault Earthquake

Eric M. Dunham and Ralph J. Archuleta

To appear in BSSA

## Abstract

Elastodynamic considerations suggest that the acceleration of ruptures to supershear velocities is accompanied by the release of Rayleigh waves along the fault from the stress breakdown zone. These waves generate a secondary slip pulse trailing the rupture front, but manifest almost entirely in ground motion perpendicular to the fault in the near-source region. We construct a spontaneously propagating rupture model exhibiting these features, and use it to explain ground motions recorded during the 2002 Denali Fault earthquake at pump station 10, located 3 km from the fault. We show that the initial pulses on both the fault normal and fault parallel components are due to the supershear stress release on the fault while the later arriving fault normal pulses result from the trailing subshear slip pulse on the fault.

## Introduction

On November 3, 2002, a  $M_w$  7.9 earthquake shook central Alaska. Rupture initiated at 22:12:41.0 UTC on the Susitna Glacier thrust fault before subsequently transferring onto the Denali fault. After propagating 240 km east on this fault, the rupture branched onto the Totschunda fault. Only one instrument, pump station 10 (PS10), maintained by the Alyeska Pipeline Service Company, recorded near-source ground motions. PS10 is located approximately 70 km east of the epicenter along the Denali fault near the Trans Alaska Pipeline. Figure 1 provides a schematic map of the fault geometry.

Finite fault inversions and geological considerations support a right-lateral strike-slip mechanism on a nearly vertical fault near PS10 (Eberhart-Phillips *et al.*, 2003). Situated only 3 km north of the fault, the station recorded a particularly interesting sequence of strong ground motion pulses as the rupture extended past it. Figure 2 shows the instrument-corrected records, which have been rotated into fault normal (FN) and parallel (FP) components (Ellsworth *et al.*, 2004).

A single one-sided pulse (labeled A in Figure 2) characterizes the FP component. The pulse is narrow (approximately 3 s rise time) and roughly symmetric. The FN component contains two similarly narrow pulses, the first (B) concurrent with A. The second (C) arrives 2.6 s later and is only slightly smaller in amplitude. Furthermore, about 6.5 s after the initial pulse, a broad motion (D) begins on the FN component, comprising of motion toward and then away from the fault.

We focus on several features. First, the FP amplitude is approximately 1.5 times larger than FN. This is not typical of large strike-slip earthquakes, as discussed by Archuleta and Hartzell (1981); Hall *et al.* (1995). As several authors have suggested (Ellsworth *et al.*, 2004; Aagaard and Heaton, 2003) and we corroborate, this is accounted for by supershear rupture speeds. However, kinematic analyses which allow slip only once at the rupture front have failed to explain pulses C and D. We show that these pulses arise naturally in dynamic models that exhibit a transition from sub-Rayleigh to supershear rupture speeds; as such, they are a uniquely transient feature not present in steady-state solutions. A consideration of the dynamics of such a transition suggests that the breakdown in stress occurring behind the rupture front releases interface waves along the weakened fault that trail the faster-moving supershear front. These are essentially Rayleigh waves dispersed by friction, although, depending on the stability of the frictional sliding and rupture pulse width, these may be accompanied by a stress drop. These interface waves cause additional slip but carry almost all of their energy in FN motion (pulse C), hence their absence from the FP component.

As is well known, mode II cracks are allowed to propagate within two steady-state velocity regimes: either below the Rayleigh wave speed (sub-Rayleigh) or between the S and P wave speeds (supershear). Propagation between the Rayleigh and S wave speeds is associated with energy generation rather than dissipation within the breakdown zone, indicating that these velocities should be rejected as unphysical. Theoretical studies suggested the possibility of supershear ruptures, beginning over three decades ago with

a study by Burridge (1973) of the self-similarly expanding mode II crack with a critical stress fracture criterion. His analytical solution showed that as a sub-Rayleigh crack extends, a peak in shear stress traveling at the S wave speed develops ahead of the crack tip. For prestress levels sufficiently close to the critical stress, this peak exceeds the critical level and could initiate a supershear rupture. This was later confirmed by the numerical experiments of Andrews (1976), which extended the fracture criterion to a more realistic condition requiring finite energy dissipation for crack growth.

Seismological observations suggest that supershear propagation has occurred, at least locally, in a number of crustal strike-slip events. Archuleta (1984) concluded that rupture velocities exceeding the S wave speed were necessary to explain records from the 1979 Imperial Valley event. Strong motion recordings of the 1999 Izmit and Düzce events suggest supershear growth, at least in one direction (Bouchon *et al.*, 2000, 2001). Waveform modeling of regional records from the 2001 Kunlunshan earthquake also indicates supershear velocities (Bouchon and Vallée, 2003).

Recent laboratory studies by Rosakis and coworkers (Rosakis *et al.*, 1999; Xia *et al.*, 2004) provided experimental verification of supershear crack growth. Several numerical (Geubelle and Kubair, 2001; Fukuyama and Olsen, 2002; Dunham *et al.*, 2003) and analytical (Huang and Gao, 2001, 2002; Samudrala *et al.*, 2002; Kubair *et al.*, 2002; Guo *et al.*, 2003) studies have focused on properties of and mechanisms for triggering supershear propagation.

## Elastodynamic Considerations

The allowed velocity regimes and supershear transition mechanism follow from a study of the waves that transmit shearing forces from within the breakdown zone to the unbroken material ahead of the rupture front. To illustrate this, we consider a semi-infinite mode II crack constrained to the plane  $y = 0$  in a homogeneous elastic medium, with fields depending on  $x$  and  $y$  only. The medium is characterized by a shear modulus  $\mu$  and P and S wave speeds  $c_p$  and  $c_s$ . At time  $t = 0$ , the crack tip, which is moving along the positive  $x$ -axis at velocity  $V$ , passes the origin.

To solve for the fields within the medium, we must specify boundary conditions on the material directly on either side of the fault. In order that the fault does not open, we require continuity of normal displacement. Continuity of shear and normal tractions across the interface follows from momentum

conservation. Furthermore, at each point on the fault, we must specify either slip or shear traction. In contrast to a kinematic source representation, in which the slip field is specified at every point on the fault, we follow the usual dynamic representation by specifying shear traction behind the moving crack tip and slip (identically zero) ahead. We require the stress field to be nonsingular at the tip, which is accomplished by introducing a finite length or time scale over which the breakdown in stress occurs, as in the cohesive zone models of Ida (1972); Palmer and Rice (1973); Andrews (1976).

We then consider an advance of the crack tip over an infinitesimal time interval  $dt$ . As the crack extends, the shear traction relaxes behind the crack tip. The exact process by which this occurs depends on the specific friction law or fracture criterion. The linearity of the governing equations allows us to construct the breakdown in stress as a superposition of line tractions (extending infinitely in the  $z$ -direction), each applied at some distance  $x = -L$  behind the crack tip with amplitude  $F$  (force/length) and having step-function time dependence. Since the shear traction at time  $t = dt$  is specified, then  $F(x) = [\sigma_{xy}(t = 0, x) - \sigma_{xy}(t = dt, x)] dx$ , where  $dx = Vdt$  and  $\sigma_{ij}$  are the components of the stress field created by slip. This is illustrated in Figure 3. The region of nonzero stress drop, in contrast to the actively slipping area in the kinematic representation, is the only source of elastic waves in the dynamic representation.

Letting  $u_i$  be the components of the displacement field created by slip, we formally define this mixed boundary value problem as

$$\begin{aligned} u_x(t, x, y = 0) &= 0 \text{ for } Vt < x < \infty \\ \sigma_{xy}(t, x, y = 0) &= -FH(t)\delta(x + L) \text{ for } -\infty < x < Vt \\ \sigma_{yy}(t, x, y = 0) &= 0 \text{ for } -\infty < x < \infty, \end{aligned} \quad (1)$$

where  $H(t)$  is the step function and  $\delta(x)$  is the delta function. The last equation, which states that the normal stress is unchanged by slip, follows from symmetry conditions that arise when requiring the continuity of both normal stress and normal displacement.

Our approach to understanding dynamic crack growth is similar to that taken by Freund (1972a,b), and our problem is related to his so-called fundamental solution in the limit that  $L \rightarrow 0$ . The advantage to keeping  $L$  finite is conceptual, affording us an insight into the elastodynamic processes occurring within the breakdown zone.

We could further generalize this model by placing the stress drop some distance off of the fault within a damage zone. In this case the superposition would be over the volume containing the off-fault damage, rather than localized to the area of the fault within the cohesive zone. Considering the problem from this perspective, the transmission of forces to the unbroken area ahead of the crack tip occurs with the broken fault behind the crack tip playing the role of an interfacial waveguide for the elastic waves emitted from within the damage zone. Since we have posed the problem within the framework of a mixed boundary value problem, the transition between the regions in which we specify shear traction and those in which we specify that slip vanishes (i.e., the crack edge), acts as a diffracting boundary. The waves released by the stress drop overtake the crack tip and diffract off of it (see Figure 4).

The solution to our problem defines the Green function for some distribution of shear tractions applied on the sliding surface of a moving crack. Known as a transient weight function, it has a known analytical solution in the Fourier-Laplace domain (Freund, 1974; Brock, 1982; Kuo and Chen, 1992; Freund, 1989; Broberg, 1999). However, since the problem possesses a characteristic length, the solution is not self-similar and requires multiple integrations to invert the transforms and extract the space-time history of the velocity and stress fields. Inversion of these transforms is, to the best of our knowledge, absent from the literature except for the use of asymptotic theorems to study the evolution of the stress intensity factor. Consequently, we present instead a numerical solution using the boundary integral methodology proposed by Geubelle and Rice (1995). The slip velocity and shear traction on the interface are shown as a function of position and time in Figure 5 for a stationary crack tip. A similar solution is obtained for sub-Rayleigh crack speeds; only when the crack velocity exceeds some wave speed does the wavefront pattern change since these waves will no longer overtake the crack tip.

Up until the arrival of the P wave at the crack tip, the solution is self-similar and identical to that of Lamb's problem (a shear line force applied on the surface of a traction-free half-space), which is used to validate the numerical method (see the inset in Figure 5). As such, the main features are well known. The line force emits P and S waves with cylindrical wavefronts, as well as planar head waves and an interfacial Rayleigh wave. A point on the fault begins to slip in the direction of the applied traction at the simultaneous arrival of the P wave and a head wave traveling along the interface at the

P wave speed. This head wave is a radiating S wave excited by evanescent P waves trapped on the fault surface. Forward sliding continues until the arrival of the S wave, at which point slip reverses, with the interface sliding in the direction opposite the applied traction. Reverse sliding ceases when the Rayleigh wave arrives; positive slip velocity peaks at and decays after its arrival, with slip reaching the steady-state value only asymptotically as is characteristic in two dimensions.

There is a direct correlation between the allowed propagation velocity regimes and the direction of slip relative to the applied traction, as pointed out by Das (2003). For a given distribution in time and space of shear tractions (i.e., a prescribed rupture history), we could calculate the slip velocity history, which would be equivalent to that generated in Lamb's problem plus a correction to account for diffractions off of the crack tip, which are further discussed below. The rate of energy dissipation at each point on the fault is the product of the shear traction and slip velocity, from which we see that only when the fault slips in the direction of the applied traction is energy dissipated. Reverse motions, which we have allowed in our problem to render it linear, are typically prevented by friction; otherwise, this process would unphysically create energy.

Let us now take the steady-state limit of our problem. In this case, it is more appropriate to consider fixing the distance  $L$  in a frame that moves with the crack tip; such an analysis was conducted by Burridge *et al.* (1979) in their study of the stability of supershear propagation velocities. In the steady-state limit, only motions for which the apparent velocity along the fault matches that of the crack tip remain (i.e., those having a ray parameter of  $V^{-1}$ ). For sub-shear propagation velocities, this implies that the driving force is carried only by evanescent P and S waves on the fault surface. A reversal in the direction of the shearing force carried by these waves occurs at the Rayleigh speed, resulting in the velocity range between the Rayleigh and S wave speeds becoming forbidden. In the supershear regime, the P wave remains evanescent but the S wave switches from evanescent to radiating. The angle that the S wavefront makes with the fault is the Mach angle  $\arcsin(c_s/V)$ . The associated shear fields retain a finite amplitude at infinity along the Mach cone. The only velocity at which the S wave vanishes is the well known  $\sqrt{2}$  times the S wave speed (Eshelby, 1949). The significance of this velocity appears clearly in the expression for the traction components on a flat surface due to incident plane waves (e.g., (Aki and Richards, 2002, p.132)). In our case, the situation is reversed, with traction changes on

the surface exciting some superposition of plane waves. Our source is the application of a shear traction, with the normal traction remaining constant. It follows from the expressions in Aki and Richards (2002) that changes in shear traction moving at  $V = \sqrt{2}c_s$  will not excite S waves.

We now return to the general transient problem and consider the diffraction pattern that emerges when steady-state conditions are not satisfied. This can occur when the crack tip accelerates between two steady-state regimes or when the magnitude of the stress drop is spatially heterogeneous. A simple illustration of this phenomenon is the growth of an initially steady-state crack into a region of increased stress drop (an asperity), as in the numerical study of Fukuyama and Olsen (2002). If we constrain the crack velocity to remain constant through this process, then the resulting fields can be constructed as a superposition of the fields carried by the original steady-state crack and the fields generated by the additional stress drop within the asperity applied some distance behind the moving crack tip, the remainder of the fault behind the tip being traction-free. This additional solution is exactly the transient diffraction problem we have solved. If we relax the constant velocity condition and allow the crack to grow spontaneously according to some fracture criterion, then provided that the additional energy released within the asperity is sufficient, the diffracted P and S waves will initiate supershear growth. If this energy is sufficiently concentrated (by an abrupt large amplitude asperity), then the crack tip will be driven forward continuously by these diffracted waves to a supershear velocity. If the asperity amplitude is smaller, yet still large enough to provide sufficient energy to power the supershear rupture, then the diffracted S wave peak will build up gradually ahead of the crack tip and the supershear transition will be discontinuous.

Another source of these transient features is the presence of an additional diffracting boundary, such as the second crack tip (see, e.g., Figure 1 of Eshelby (1969)) or the healing front in a rupture pulse model. The multiple diffractions between the two expanding crack tips generate the S wave stress peak that appears in analytical self-similar solutions for sub-Rayleigh cracks (Burridge, 1973; Broberg, 1994, 1995; Freund, 1989; Broberg, 1999). The supershear transition appearing in the numerical experiments of Andrews (1976) on a bilaterally extending crack with homogeneous stress drop occurs by this mechanism. For an expanding crack, these diffractions have significant amplitude only during nucleation, where the characteristic length controlling the development of these features is the nucleation zone size, as found by Andrews (1976). In this case the S wave peak builds up gradu-

ally, resulting in a discontinuous triggering of the supershear rupture some distance ahead of the original sub-Rayleigh rupture.

For supershear propagation velocities, the Rayleigh and S waves released within the breakdown zone will not overtake the crack tip. As self-similar analytical solutions in this velocity regime reveal (Burrige, 1973; Broberg, 1994, 1995), slip is not concentrated uniquely at the rupture front, as it is for sub-Rayleigh ruptures. A second peak in slip velocity travels at the Rayleigh speed. Similarly, spontaneously propagating cracks that accelerate from sub-Rayleigh to supershear velocities leave behind a secondary slip pulse at the Rayleigh speed. This feature emerges naturally from our representation of crack growth as Rayleigh waves generated within the breakdown zone that never reach the faster-moving crack tip. If the supershear transition is triggered by an asperity, then these Rayleigh waves derive their energy from the additional stress release within the asperity. As we later discuss, the signature of these Rayleigh waves in seismic radiation manifests almost entirely in ground motions perpendicular to the fault plane.

The effect of friction on the fault will be to disperse these Rayleigh waves. The dispersion relation for a linearized version of rate and state friction is given by Rice *et al.* (2001). Depending on frictional parameters and sliding conditions, larger wavelengths may unstably grow into the nonlinear regime until a stress drop occurs. In this way, the Rayleigh wave could be viewed as a secondary rupture.

Extension of this analysis to three dimensional crack propagation is complicated. The representation of the breakdown zone consists of a superposition of point shear tractions applied some distance behind an arbitrarily shaped moving crack edge. Curvature of the crack edge focuses or defocuses the radiation released by the tractions (Achenbach and Harris, 1978). Such focusing alone can be sufficient to trigger localized supershear bursts (Dunham *et al.*, 2003). Furthermore, the driving force provided by the stress drop becomes directionally dependent. Including friction and rotation of the slip vector introduces another nonlinearity into the problem. An exact solution for a point stress drop in three dimensions, neglecting any diffractions but including a linearized treatment of rake rotation under constant friction, is given by Dunham (2004).

# Spontaneous Modeling

We construct a simple rupture model exhibiting a transition from sub-Rayleigh to supershear propagation, and show that the ground motion explains several features recorded at PS10. We use a staggered-grid finite difference code with second order explicit time stepping (Favreau *et al.*, 2002). The method converges spatially at eighth order away from the fault and has perfectly matched layer absorbing boundaries on all sides, except the free surface, to prevent artificial reflections from contaminating the solution. Slip is constrained to be horizontal, rendering the dynamics insensitive to the absolute stress level. Reverse slip is prohibited.

Since the station is located only 3 km from the Denali fault and many tens of kilometers from the Susitna Glacier and Totschunda faults, we model the rupture process on only one straight fault segment. The dynamic inverse problem pushes the limits of current computational capabilities (Peyrat and Olsen, 2004), so we use trial and error forward modeling. For simplicity, and to demonstrate that a supershear transition is the only feature required to match the ground motion, we assume that all material and frictional properties are uniform with depth.

We use a simple friction law that exhibits both slip-weakening and healing behaviors. The two parameter law requires that a slip-weakening distance  $D$  and healing time  $T$  be specified at each point on the fault. We define the non-dimensionalized stress as  $\theta = (\sigma_{xy} - \sigma_f)/(\sigma_y - \sigma_f)$ , where  $\sigma_y$  and  $\sigma_f$  are the yield stress and sliding friction. The stress evolves following

$$\dot{\theta} = -\frac{\theta \delta v}{D} + \frac{1 - \theta}{T} \quad (2)$$

once the fault begins to slip. Slip velocity is defined as  $\delta v = v_x(y = 0^+) - v_x(y = 0^-)$  and reverse slip is forbidden. This friction law was introduced by Nielsen and Carlson (2000), and provides a convenient way to include healing. For  $T \rightarrow \infty$ , it reduces to an exponential slip-weakening law. Note that the slip-weakening distance  $D$  for this model is twice that used in the standard linear slip-weakening model (Andrews, 1976) having the same fracture energy.

We artificially nucleate the rupture by slightly overstressing a region 61 km from the station, chosen to match the distance to the intersection of the Susitna Glacier and Denali faults. As several models have suggested (Harris *et al.*, 1991; Harris and Day, 1993; Kase and Kuge, 1998; Magistrale and Day, 1999; Anderson *et al.*, 2003), ruptures jump between faults almost exclusively

when the initial rupture reaches the edge of the original fault. Dynamic modeling of the transfer from the Susitna Glacier to Denali fault by Aagaard *et al.* (2004) suggests that this occurs about 10 s after initiation. The arrival time of pulses A and B then places a lower bound on the average rupture velocity from the intersection of the faults to PS10 of  $0.75c_s$ , neglecting any time spent during nucleation on the Denali fault. Assuming that pulses A and B are associated with a supershear rupture (propagating at about  $1.5c_s$ ) and pulse C with a Rayleigh wave, then the separation in time between these pulses requires the supershear transition to have occurred about 30 km before PS10. Combined with the assumption that slip transfers from the Susitna Glacier fault to the Denali fault about 10 s after nucleation (Aagaard *et al.*, 2004), we estimate an initial sub-Rayleigh rupture speed of about  $0.5\text{-}0.6c_s$ . In our models, the rupture begins bilaterally on the Denali fault, but we introduce a barrier 10 km to the west, consistent with surface slip measurements (Eberhart-Phillips *et al.*, 2003), that arrests propagation in that direction. The initial stress level is selected such that the rupture is sub-Rayleigh, and no healing is used initially.

We distinguish between two types of supershear transitions observed in our simulations. In the first, the S wave stress peak that triggers the transition is released during nucleation (as in Andrews (1976)). Even for a properly resolved nucleation process with the slip-weakening laws used, an overestimate of the critical crack length (due to using an inappropriately large value of the slip-weakening distance) will result in a physically premature transition. If ruptures nucleate from much smaller patches and the slip-weakening distance that governs fully dynamic propagation is much larger than that governing nucleation (as experimental and numerical work indicates), then numerical results exhibiting this type of transition are incorrect. Instead, a preferable type of transition would be one in which nucleation generates a negligible shear diffraction peak and some other process, such as growth into a region of increased stress drop (Fukuyama and Olsen, 2002) or focusing by rupture front curvature (Dunham *et al.*, 2003), builds the peak to a critical level. To ensure this, we trigger the supershear transition by increasing the initial stress level in an asperity beginning about 30 km from the hypocenter (see Figure 6), and make sure that diffractions from the nucleation process have negligible influence on rupture growth.

The short rise times at PS10 are inconsistent with a traditional crack model, indicating that the actively slipping region is quite narrow, as appears to be typical in the earth (Aki, 1968; Archuleta and Day, 1980; Heaton, 1990).

Several mechanisms are known to generate rupture pulses, which are recognized as an alternative and equally valid solution to the elastodynamic equation (Freund, 1979; Broberg, 1999; Nielsen and Madariaga, 2004). Strong slip rate weakening is one possibility (Cochard and Madariaga, 1994; Madariaga and Cochard, 1994; Perrin *et al.*, 1995; Zheng and Rice, 1998). A friction law containing restrengthening on a short time scale can also generate rupture pulses (Nielsen and Carlson, 2000). Rupture pulses also result from interaction with geometrical heterogeneities, such as strength heterogeneities or fault borders that transmit arrest phases to initiate healing (Archuleta and Day, 1980; Day, 1982; Johnson, 1990; Beroza and Mikumo, 1996).

We present three models. The first (I) allows slip to 10 km depth and lacks healing. With these constraints, we were unable to match the short rise time on the FP component. Decreasing the slip-weakening distance does not alter the FP rise time, and actually makes FN pulse B too narrow. Instead, we tried two approaches to decrease the rise time. Our second model (II) allows slip to 10 km depth but adds a healing time of order one second (only within the asperity region). In these first two models, a healing front emanates from the western side of the Denali fault when the rupture arrests there, creating a rupture pulse about 16 km wide. The pulse width remains constant until the rupture encounters the region of high prestress, where the supershear transition begins. The third model (III) lacks healing, but restricts slip to 5 km depth. In this case, the rupture pulse width is about 8 km, and is controlled by the fault width rather than by the stopping phase from the western end of the fault. The model parameters and fault geometry are summarized in Table 1 and Figure 6. Snapshots of the rupture history of our models are shown in Figure 7 and Movies 1-3. Figure 8 compares our synthetics to the corrected data. We allow a linear shift in time since the nucleation process is artificial. We scale the amplitude of our synthetics to match pulse A identically; this sets the magnitude of the stress drop  $\sigma_y - \sigma_f$  (Table 1).

Let us begin with model I. When the rupture enters the region of increased prestress, the transient diffractions appear and accelerate the rupture from  $0.65c_s$  to  $1.6c_s$ . It continues at the supershear velocity as it passes the station. The supershear rupture takes the form of a pulse of expanding width, with the healing front trailing at the S wave speed. The fault is locked after this healing front until the Rayleigh arrival, in accordance with the elastodynamic considerations discussed previously. This corresponds to the forbidden velocity region that occurs when the slip direction attempts to reverse itself.

Our theoretical model also predicts a Rayleigh wave behind the supershear front, which manifests itself here as a secondary slip pulse. This model gives too large of a rise time on FP to be consistent with the data. In contrast, we find the width of FN pulses B and C to be far less sensitive to the slip duration. However, the dip in amplitude between these pulses is controlled by the slip duration, and the strong dip seen in the data suggests that the fault has negligible slip between the supershear rupture front and the secondary Rayleigh rupture pulse.

There are several features that are not predicted by the two dimensional theoretical model, which neglects both the finite width of the fault and the free surface. The propensity of ruptures near the free surface to become supershear has been noted by several researchers (Aochi, 2002; Gonzalez, 2003), and is related to phase conversion at the free surface. This phenomenon can be seen in Figure 7 and Movies 1-3, in which the supershear rupture front emerges at the free surface and spreads laterally down the rupture front. Note also the change in the slip velocity pattern across a line extending back from where the rupture front meets the free surface, as well as where it intersects the bottom edge of the fault (particularly evident in the last several snapshots). The angle that this line makes with the horizontal is the S wave Mach angle, indicating that behind this wavefront, S waves converted by the free surface cause increased slip velocity.

In model II, we add frictional healing to decrease the rupture pulse width. In this case, the healing front follows at approximately the same speed as the supershear rupture front. To match the short rise time of pulse A requires a healing time  $T$  of order one second (Table 1). This generates a complicated stress history on the fault because there is an additional stress drop associated with the secondary slip pulse. Healing raises the stress levels such that a sufficiently large perturbation (provided by the Rayleigh wave) destabilizes the frictional sliding to generate a secondary rupture. This does not occur in the previous model, where the secondary slip pulse is closer to a true Rayleigh wave that propagates without altering the fault tractions. However, the healing is too strong for the secondary pulse to persist, and it dies out after propagating about 30 km.

This healing time does not necessarily imply a rapid restrengthening, but may be interpreted as evidence of a characteristic time arising from some unmodeled source process that locks the fault. Such a value could be related to a smaller length scale characterizing strength or stress heterogeneities, which has been shown to control the rupture pulse width (Beroza and Mikumo,

1996). We test this hypothesis in model III, which introduces the smaller length scale simply by limiting slip to 5 km depth. This achieves a comparably short rise time without the use of healing. In this case, the rupture pulse width is controlled by the fault depth, as in Day (1982). The healing front moves at the same speed as the supershear rupture front.

The amplitude and duration of pulses A, B, and C are well matched for models II and III. The simplicity of our models allows us to explain the relationship between fault processes and the ground motion pulses. We show the evolution of FP and FN ground motions for model III as the rupture transitions to supershear velocities in Figure 9, and for all models in Movies 4-9. We also present seismograms for this model at hypothetical stations before and after PS10 in Figure 10, which highlight the fact that the PS10 record exhibits characteristics of both supershear and sub-Rayleigh ruptures.

Before encountering the high stress region, the radiation pattern is characteristic of steady-state sub-Rayleigh ruptures in that FN dominates FP in amplitude. The FP radiation pattern is characterized by four lobes (nodal on the fault plane) that give rise to two one-sided pulses recorded at a fixed receiver. The pattern is effectively that of a dislocation source. On the right-moving block, the FN motion preceding the rupture is away from the fault and trailing the rupture is in toward the fault. This results in the typical two-sided FN pulse. These characteristic motions are discussed by Archuleta and Hartzell (1981); Hall *et al.* (1995) and were observed, for example, in the 1966 Parkfield earthquake (Aki, 1968). As the rupture pulse length increases (approaching a crack model), the two trailing lobes on FP coalesce into a large tail. In addition, the downward FN motion arrives later and diminishes in amplitude. The downward motion is thus directly associated with the passage of the healing front.

Evidence of the supershear transition on the FP component comes as the rupture begins to outrun the S waves, which ultimately lie behind a planar wavefront emanating from the rupture front in a Mach cone. Arrival of this wavefront gives rise to the large one-sided pulse (A). The amplitude of this feature increases as the supershear rupture develops, until its amplitude dominates the FP motions (see Figure 10). In addition to the planar shear wavefront, the fully developed supershear rupture possesses a two-lobed pattern preceding the main shear wavefronts that must arise from P waves. The lack of a preliminary bump preceding pulse A indicates that the rupture was not in steady-state conditions as it passed the station. The small rise and plateau before pulse A arrives much too early to be an indication of this fea-

ture. The trailing Rayleigh wave has negligible signature in the FP ground motion.

The pattern of FN ground motion associated with the supershear transition is more complex. A pair of one-sided pulses, with motion away from the fault on the right-moving block, begin to emanate from the supershear rupture front along the planar S wavefronts. These grow in amplitude as steady-state supershear conditions are reached and correspond to pulse B. Note that the motion actually peaks slightly before FP pulse A, consistent with the observations. This is because the motion actually precedes the Mach cone. This motion decreases to a minimum between pulses B and C. Pulse C corresponds to the Rayleigh wave, and is similar in characteristic to a typical subshear rupture. The dip between these peaks likely indicates that the fault has no significant slip between the supershear rupture front and the Rayleigh wave. The amplitude of the trailing Rayleigh wave is particularly sensitive to the frictional evolution of the fault. If accompanied by too large of a stress drop (as could occur if the fault rapidly restrengthens), the Rayleigh wave develops into a strong secondary rupture, accompanied by an amplitude increase in these later motions. Also, if the triggering prestress is too large, the majority of the energy goes into supershear motions at the expense of the Rayleigh pulse. This places a strong constraint on the triggering prestress in our models, and we find it to be just barely above the minimum required to initiate the supershear transition.

We did not find it possible to exactly fit the negative FN pulse D. A similar negative motion appears after the passage of a dislocation, and is associated with the healing front in a rupture pulse model. An examination of the rupture histories shows that our models exhibit an extremely narrow Rayleigh rupture pulse that causes the negative FN pulse to arrive immediately after pulse C. We speculate that pulse D corresponds to the passage of a healing front associated with a Rayleigh pulse roughly twice as wide as observed in our models. In our models, the Rayleigh wave is likely to be narrow because finite difference methods have difficulty resolving surface waves. Furthermore, broadening of the Rayleigh wave could also occur due to frictional dispersion, as is characteristic of any friction law possessing intrinsic time or length scales. Further work is needed to test this hypothesis, but if true, then this record could provide valuable constraints on the frictional properties of slipping faults.

## Discussion

We have analyzed strong ground motion recordings from the 2002 Denali Fault earthquake and conclude that they provide evidence of supershear rupture propagation past PS10. A study of the waves generated within the stress breakdown zone behind the rupture front sheds light on how the forces that drive supershear propagation are transmitted to the unbroken region ahead of the rupture front. As noted by Ellsworth *et al.* (2004), a supershear rupture leads to large amplitudes on both the FP and FN components of motion. Rupture growth into a region of increased stress drop triggers a set of transient diffractions that accelerate the rupture from sub-Rayleigh to supershear velocities. This process is accompanied by the release of a Rayleigh wave on the fault surface. This appears as a secondary slip pulse that manifests itself primarily in FN ground motion, explaining late arriving FN pulses recorded at PS10 that are not explained in supershear kinematic models. The separation in time of these FN pulses indicates that the supershear transition occurred about 30 km before PS10.

While our models show persistent supershear rupture well after PS10, this is not required by the records of PS10 and occurs only because the high prestress level used to trigger supershear growth is maintained thereafter. To place a lower bound on the supershear propagation distance required to match the PS10 record, we limited the width of the high stress region (Figure 6). We found that a minimum width of about 35 km is required to match the records. In this case, the supershear rupture is transient. It persists beyond the high stress region and dies out about 30 km past PS10. When the secondary Rayleigh rupture pulse encounters this region, it resumes its role as the only rupture front.

The narrow width of pulse A and the strong dip in amplitude between pulses B and C are incompatible with a traditional crack model, indicating that the supershear rupture took the form of a narrow slip pulse. The same cannot be concluded for the secondary Rayleigh rupture pulse, which we speculate was about twice as broad as the pulse observed in our simulations. Our dynamic models demonstrate that a narrow supershear pulse could arise either from frictional healing over a time scale of 1.5 s or from the presence of a 5 km length scale characterizing the stress distribution. While the rupture histories of these models differ (Figure 7 and Movies 1-3), the resulting ground motion at PS10 is nearly identical (Figure 8). In light of this, we emphasize that our models should not be interpreted as provid-

ing an exact slip history of the fault, which cannot be determined uniquely from one record. Instead, our models contain only the minimum number of parameters required to explain the main features of the record.

The multiple slip pulses that we observe in our dynamic models highlight the difficulty kinematic models may have when fitting or inverting data that result from supershear ruptures, particularly if supershear growth occurs in transient bursts. Dynamical inversion efforts like those by Peyrat and Olsen (2004), while presently extremely expensive computationally, are a possible future solution.

## Acknowledgements

We sincerely thank Pascal Favreau for providing us with the finite difference code used in this study. We thank Michel Bouchon and Martin Vallée for their constructive reviews. This project was supported by the David and Lucile Packard Foundation, NSF Grant No. DMR-9813752, and by a grant from the Keck Foundation which established an Interdisciplinary Program in Seismology and Materials Science at UCSB. E.M.D. acknowledges the support of a National Defense Science and Engineering Graduate Research fellowship and the encouragement of Jean Carlson. R.J.A. was partially supported by the NSF/USGS Southern California Earthquake Center. This is ICS contribution #0643.

## References

- Aagaard, B., G. Anderson, and K. W. Hudnut (2004). Dynamic rupture modeling of the transition to strike-slip motion in the 2002 Denali Fault, Alaska, earthquake, *Bull. Seism. Soc. Am.* submitted.
- Aagaard, B., and T. H. Heaton (2003). How do near-source ground motions change when ruptures go supershear? *Eos Trans. AGU* 84, Fall Meet. Suppl., Abstract S42H-08.
- Achenbach, J. D., and J. G. Harris (1978). Ray method for elastodynamic radiation from a slip zone of arbitrary shape, *J. Geophys. Res.* 83, 2283–2291.

- Aki, K. (1968). Seismic displacements near a fault, *J. Geophys. Res.* 73, 5359–5376.
- Aki, K., and P. G. Richards (2002). *Quantitative Seismology*, University Science Books, Sausalito, California.
- Anderson, G., B. Aagaard, and K. Hudnut (2003). Fault interactions and large complex earthquakes in the Los Angeles area, *Science* 302, 1946–1949.
- Andrews, D. J. (1976). Rupture velocity of plane strain shear cracks, *J. Geophys. Res.* 81, 5679–5687.
- Aochi, H. (2002). personal communication.
- Archuleta, R. J. (1984). A faulting model for the 1979 Imperial Valley earthquake, *J. Geophys. Res.* 89, 4559–4585.
- Archuleta, R. J., and S. M. Day (1980). Dynamic rupture in a layered medium: an example, the 1966 Parkfield earthquake, *Bull. Seism. Soc. Am.* 70, 671–690.
- Archuleta, R. J., and S. H. Hartzell (1981). Effects of fault finiteness on near-source ground motion, *Bull. Seism. Soc. Am.* 71, 939–957.
- Beroza, G., and T. Mikumo (1996). Short slip duration in dynamic rupture in the presence of heterogeneous fault properties, *J. Geophys. Res.* 101, 22,449–22,460.
- Bouchon, M., M. P. Bouin, H. Karabulut, M. N. Toksöz, M. Dietrich, and A. Rosakis (2001). How fast is rupture during an earthquake? New insights from the 1999 Turkey earthquakes, *Geophys. Res. Lett.* 28, 2723–2726.
- Bouchon, M., M. N. Toksöz, H. Karabulut, M. P. Bouin, M. Dietrich, M. Aktar, and M. Edie (2000). Seismic imaging of the Izmit rupture inferred from the near-fault recordings, *Geophys. Res. Lett.* 27, 3013–3016.
- Bouchon, M., and M. Vallée (2003). Observation of long supershear rupture during the magnitude 8.1 Kunlunshan earthquake, *Science* 301, 824–826.
- Broberg, K. B. (1994). Intersonic bilateral slip, *Geophys. J. Int.* 119, 706–714.

- Broberg, K. B. (1995). Intersonic mode II crack expansion, *Arch. Mech.* 47, 859–871.
- Broberg, K. B. (1999). *Cracks and Fracture*, Academic Press, London.
- Brock, L. M. (1982). Shear and normal impact loadings on one face of a narrow slit, *Int. J. Solid Structures* 18, 467–477.
- Burridge, R. (1973). Admissible speeds for plane-strain shear cracks with friction but lacking cohesion, *Geophys. J. Roy. Astr. Soc.* 35, 439–455.
- Burridge, R., G. Conn, and L. B. Freund (1979). The stability of a rapid mode II shear crack with finite cohesive traction, *J. Geophys. Res.* 85, 2210–2222.
- Cochard, A., and R. Madariaga (1994). Dynamic faulting under rate-dependent friction, *Pure Appl. Geophys.* 142, 419–445.
- Das, S. (2003). Dynamic fracture mechanics in the study of the earthquake rupturing process: Theory and observation, *J. Mech. Phys. Solids* 51, 1939–1955.
- Day, S. (1982). Three-dimensional finite difference simulation of fault dynamics: Rectangular faults with fixed rupture velocity, *Bull. Seism. Soc. Am.* 72, 705–727.
- Dunham, E. M. (2004). Dissipative interface waves and the transient response of a three dimensional sliding interface with coulomb friction, *J. Mech. Phys. Solids* in press.
- Dunham, E. M., P. Favreau, and J. M. Carlson (2003). A supershear transition mechanism for cracks, *Science* 299, 1557–1559.
- Eberhart-Phillips, D., P. J. Haeussler, J. T. Freymueller, A. D. Frankel, C. M. Rubin, P. Craw, N. A. Ratchkovski, G. Anderson, G. A. Carver, A. J. Crone, T. E. Dawson, H. Fletcher, R. Hansen, E. L. Hard, R. A. Harris, D. P. Hill, S. Hreinsdottír, R. W. Jibson, L. M. Jones, R. Kayen, D. K. Keefer, C. F. Larsen, S. C. Moran, S. F. Personius, G. Plafker, B. Sherrod, K. Sieh, N. Sitar, and W. K. Wallace (2003). The 2002 Denali fault earthquake, Alaska: A large magnitude, slip-partitioned event, *Science* 300, 1113–1118.

- Ellsworth, W. L., M. Celebi, J. R. Evans, E. G. Jensen, D. J. Nyman, and P. Spudich (2004). Processing and modeling of the pump station 10 record from the November 3, 2002, Denali fault, Alaska earthquake, *Proceedings, 11th Intern. Conf. Soil Dynam. Earthq. Eng.* 1, Berkeley, California, pp. 471–477
- Eshelby, J. D. (1949). Uniformly moving dislocations, *Proc. Phys. Soc. A* 62, 307–314.
- Eshelby, J. D. (1969). The elastic field of a crack extending non-uniformly under general antiplane loading, *J. Mech. Phys. Solids* 17, 177–199.
- Favreau, P., M. Campillo, and I. R. Ionescu (2002). Initiation of shear instability in three-dimensional elastodynamics, *J. Geophys. Res.* 107, 2147–2164.
- Freund, L. B. (1972a). Crack propagation in an elastic solid subjected to general loading-I. Constant rate of extension, *J. Mech. Phys. Solids* 20, 129–140.
- Freund, L. B. (1972b). Crack propagation in an elastic solid subjected to general loading-II. Non-uniform rate of extension, *J. Mech. Phys. Solids* 20, 141–152.
- Freund, L. B. (1974). The stress intensity factor due to normal impact loading on the faces of a crack, *Int. J. Solid Structures* 12, 179.
- Freund, L. B. (1979). The mechanics of dynamic shear crack propagation, *J. Geophys. Res.* 84, 2199–2209.
- Freund, L. B. (1989). *Dynamic Fracture Mechanics*, Cambridge University Press, Cambridge.
- Fukuyama, E., and K. B. Olsen (2002). A condition for super-shear rupture propagation in a heterogeneous stress field, *Pure Appl. Geophys.* 157, 2047–2056.
- Geubelle, P. H. and D. V. Kubair (2001). Intersonic crack propagation in homogeneous media under shear-dominated loading: numerical analysis, *J. Mech. Phys. Solids* 49, 571–587.

- Geubelle, P. H. and J. R. Rice (1995). A spectral method for three-dimensional elastodynamic fracture problems, *J. Mech. Phys. Solids* 43, 1791–1824.
- Gonzalez, S. (2003). Foam rubber and numerical simulations of near-fault seismic directivity, Master’s thesis, San Diego State University. pp. 40-41.
- Guo, G., W. Yang, Y. Huang, and A. J. Rosakis (2003). Sudden deceleration or acceleration of an intersonic shear crack, *J. Mech. Phys. Solids* 51, 311–331.
- Hall, J. F., T. H. Heaton, M. W. Halling, and D. J. Wald (1995). Near-source ground motion and its effects of flexible buildings, *Earthq. Spectra* 11, 569–605.
- Harris, R. A., R. J. Archuleta, and S. M. Day (1991). Fault steps and the dynamic rupture process: 2-D numerical simulations of a spontaneously propagating shear fracture, *Geophys. Res. Lett.* 18, 893–896.
- Harris, R. A., and S. M. Day (1993). Dynamics of fault interaction: Parallel strike-slip faults, *J. Geophys. Res.* 98, 4461–4472.
- Heaton, T. H. (1990). Evidence for and implications of self-healing pulses of slip in earthquake rupture, *Phys. Earth Planet. In.* 64, 1–20.
- Huang, Y., and H. Gao (2001). Inter-sonic crack propagation - part I: The fundamental solution, *J. Appl. Mech.* 68, 169–175.
- Huang, Y., and H. Gao (2002). Inter-sonic crack propagation - part II: Suddenly stopping crack, *J. Appl. Mech.* 69, 76–80.
- Ida, Y. (1972). Cohesive force across the tip of a longitudinal shear crack and Griffith’s specific surface energy, *J. Geophys. Res.* 77, 3796–3805.
- Johnson, E. (1990). On the initiation of unilateral slip, *Geophys. J. Int.* 101, 125–132.
- Kase, Y., and K. Kuge (1998). Numerical simulation of spontaneous rupture processes on two non-coplanar faults; the effect of geometry on fault interaction, *Geophys. J. Int.* 135, 911–922.

- Kubair, D. V., P. H. Geubelle, and Y. Y. Huang (2002). Intersonic crack propagation in homogeneous media under shear-dominated loading: theoretical analysis, *J. Mech. Phys. Solids* 50, 1547–1564.
- Kuo, M. K., and T. Y. Chen (1992). The Wiener-Hopf technique in elastodynamic crack problems with characteristic lengths in loading, *Eng. Fract. Mech.* 42, 805–813.
- Madariaga, R., and A. Cochard (1994). Seismic source dynamics, heterogeneity and friction, *Ann. Geophys.* 37, 1349–1375.
- Magistrale, H., and S. Day (1999). Three-dimensional simulations of multi-segment thrust fault rupture, *Geophys. Res. Lett.* 26, 2093–2096.
- Nielsen, S., and J. M. Carlson (2000). Rupture pulse characterization: Self-healing, self-similar, expanding solutions in a continuum model of fault dynamics, *Bull. Seism. Soc. Am.* 90, 1480–1497.
- Nielsen, S., and R. Madariaga (2004). On the self-healing fracture mode, *Bull. Seism. Soc. Am.* 93, 2375–2388.
- Palmer, A. C., and J. R. Rice (1973). The growth of slip surfaces in the progressive failure of overconsolidated clay, *Proc. Roy. Soc. London A* 332, 527–548.
- Perrin, G., J. R. Rice, and G. Zheng (1995). Self-healing slip pulse on a frictional interface, *J. Mech. Phys. Solids* 43, 1461–1495.
- Peyrat, S., and K. B. Olsen (2004). Nonlinear dynamic rupture inversion of the 2000 Western Tottori, Japan, earthquake, *Geophys. Res. Lett.* in press.
- Rice, J. R., N. Lapusta, and K. Ranjith (2001). Rate and state dependent friction and the stability of sliding between elastically deformable solids, *J. Mech. Phys. Solids* 49, 1865–1898.
- Rosakis, A. J., O. Samudrala, and D. Coker (1999). Cracks faster than the shear wave speed, *Science* 284, 1337–1340.
- Samudrala, O., Y. Huang, and A. J. Rosakis (2002). Subsonic and intersonic shear rupture of weak planes with a velocity weakening cohesive zone, *J. Geophys. Res.* 107, doi:10.1029/2001JB000460.

Xia, K., A. J. Rosakis, and H. Kanamori (2004). Laboratory earthquakes: The sub-Rayleigh-to-supershear transition, *Science* 303, 1859–1861.

Zheng, G., and J. R. Rice (1998). Conditions under which velocity-weakening friction allows a self-healing versus a cracklike mode of rupture, *Bull. Seism. Soc. Am.* 88, 1466–1483.

parameter	model I	model II	model III
$\mu$		32.4 GPa	
$c_s$		3.4 km/s	
$c_p$		5.89 km/s	
grid spacing		125 m	
time step		4.09 ms	
distance to station		61 km	
distance to asperity $L_a$	24.375 km	27.375 km	28.75 km
fault width	10 km	10 km	5 km
$\theta$ (outside asperity)	0.45	0.45	0.7
$\theta$ (within asperity)	0.7	0.77	0.87
$\sigma_y - \sigma_f$	28.4 MPa	40.0 MPa	31.5 MPa
$D$	1.43 m	2.01 m	1.58 m
$T$	$\infty$	1.47 s	$\infty$

Table 1: Parameters for our three models.

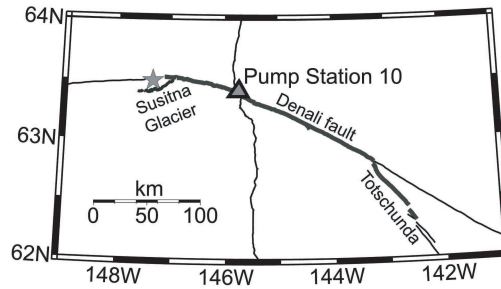


Figure 1: Fault geometry around PS10 (after Ellsworth *et al.* (2004)).

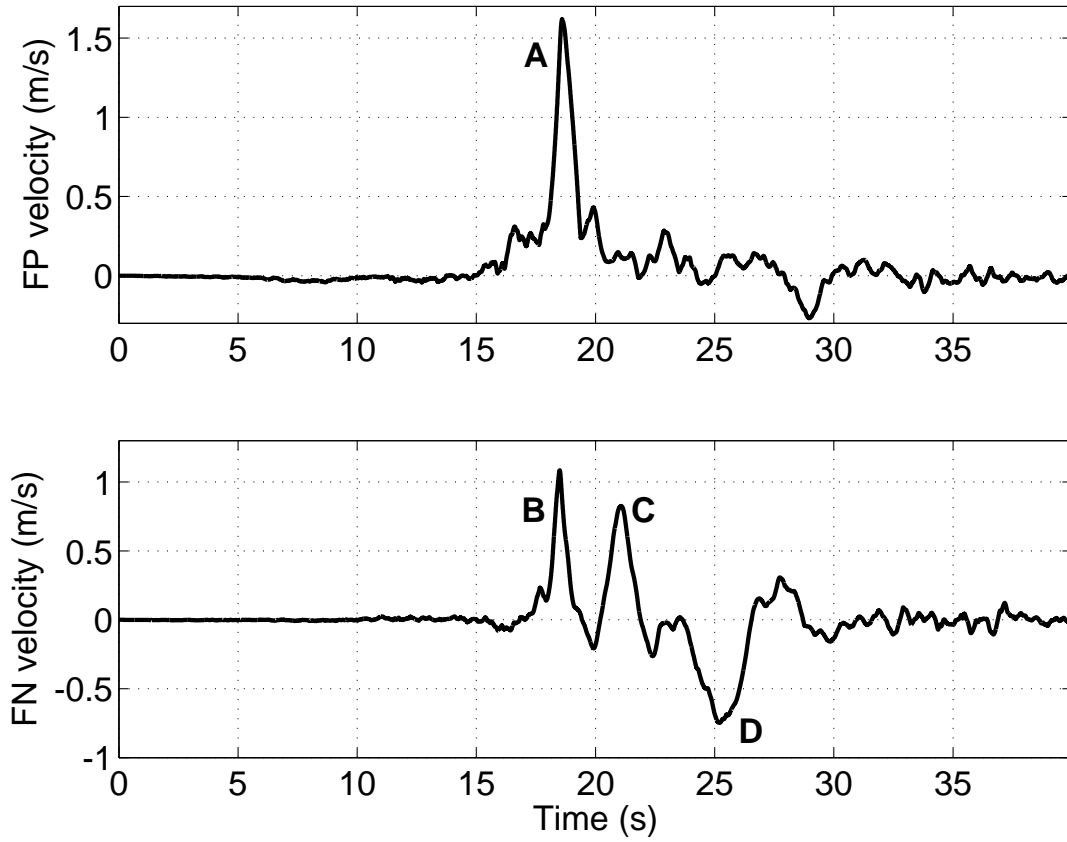


Figure 2: Instrument-corrected ground motions for PS10. The main velocity pulses are labeled to clarify discussion in the text. The record begins at the P wave arrival from the thrust event at 22:12:56.36 UTC (Ellsworth *et al.*, 2004).

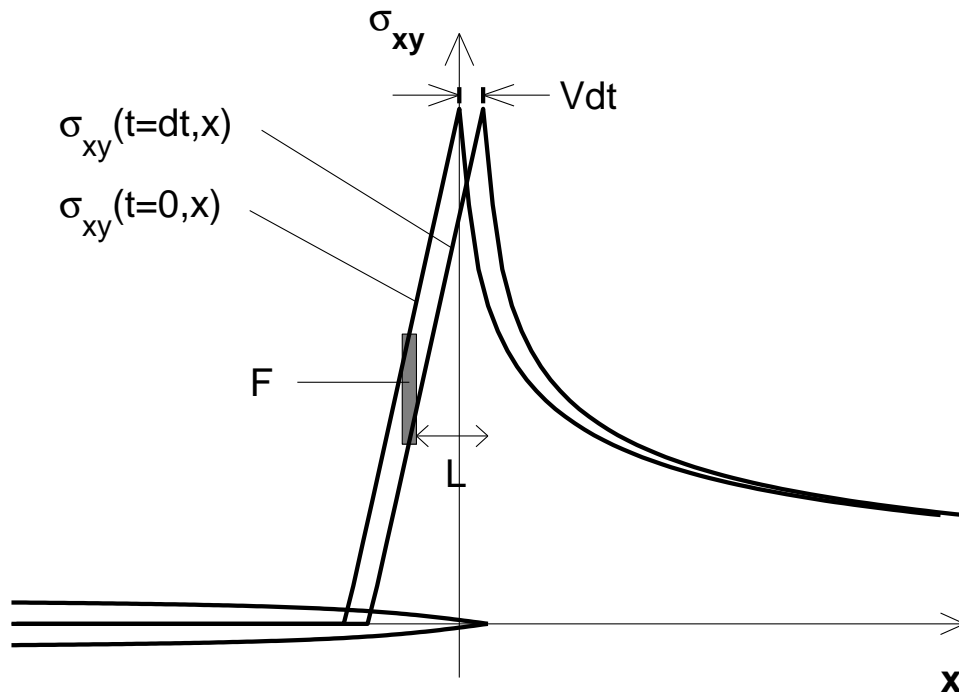


Figure 3: Schematic diagram illustrating the superposition of line tractions (stress drops) for  $x < 0$ . The fault is locked for  $x > 0$  and the crack advances at velocity  $V$  over an infinitesimal time interval  $dt$ .

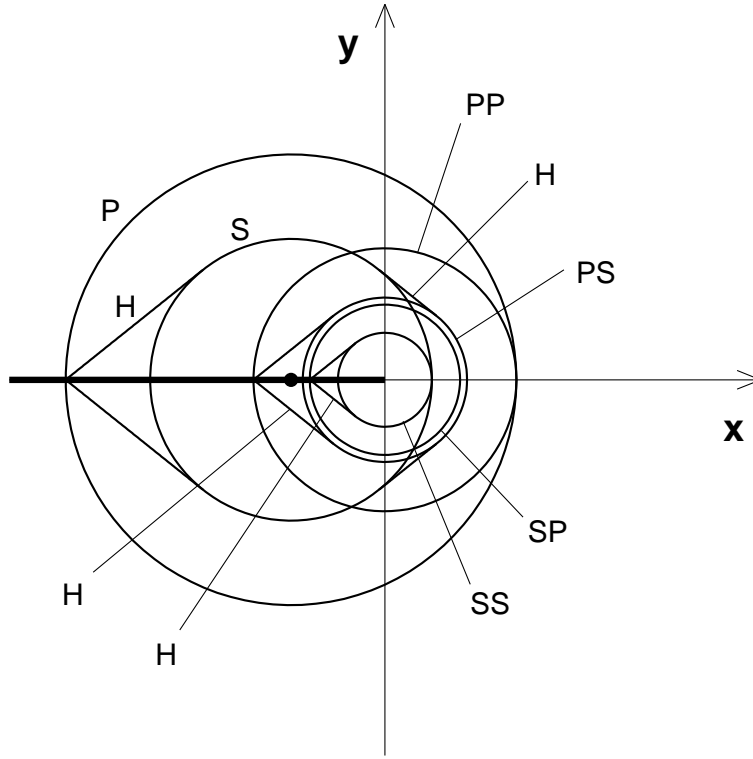


Figure 4: Wavefronts generated by a stress drop (marked by the circle) located some distance behind a stationary crack tip, after both P and S waves overtake the crack tip. Rayleigh waves and body waves generated by Rayleigh waves diffracting off of the crack tip are not shown to avoid excessive complication. The crack, denoted by the heavy line, lies in the half-plane  $y = 0$ ,  $x < 0$ . Direct and diffracted waves are labelled, and H denotes a head wave resulting from P to S conversion on the crack face.

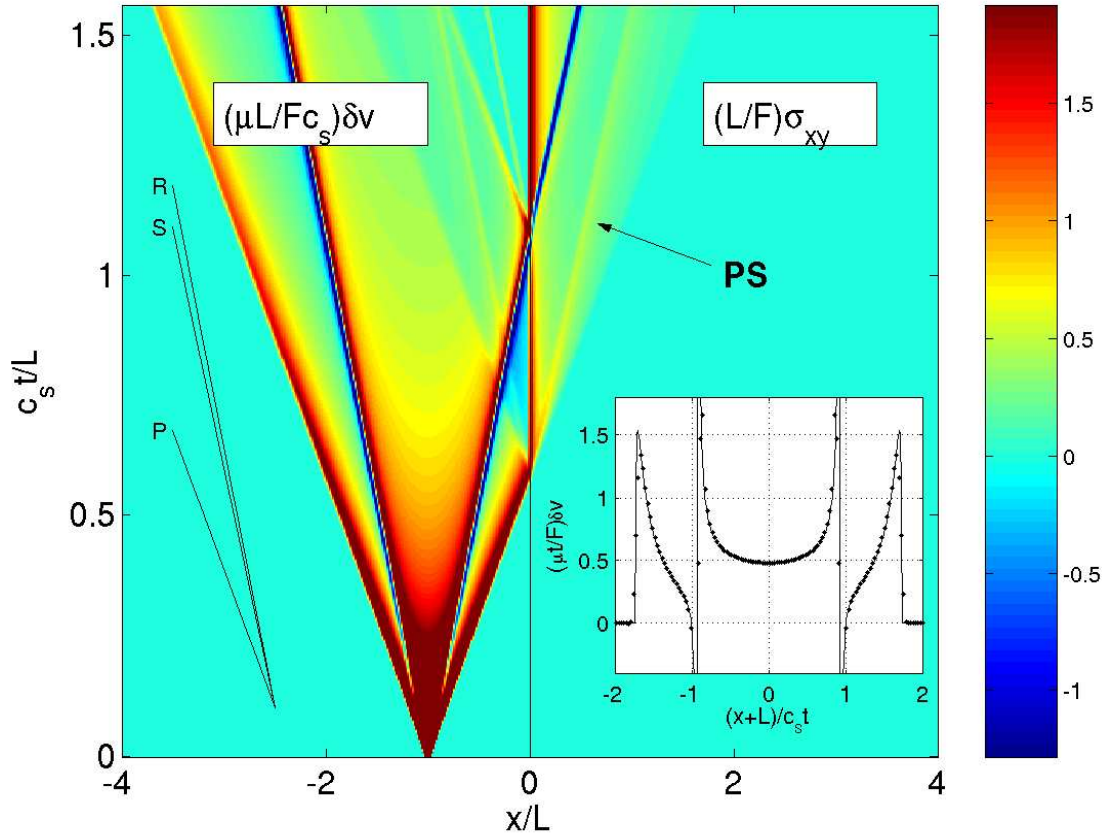


Figure 5: Evolution of slip velocity ( $x < 0$ ) and shear traction ( $x > 0$ ) after the step-function application of a line stress drop of magnitude  $F$  at  $x = -L$  behind a stationary crack tip. The color scale measures the non-dimensionalized slip velocity and shear traction labeled at the top. The inset compares the numerical slip velocity (points) just prior to wave arrivals at the crack tip to the analytical solution for Lamb's problem (solid line). The peak in shear traction associated with the P to S wave conversion is labeled PS.

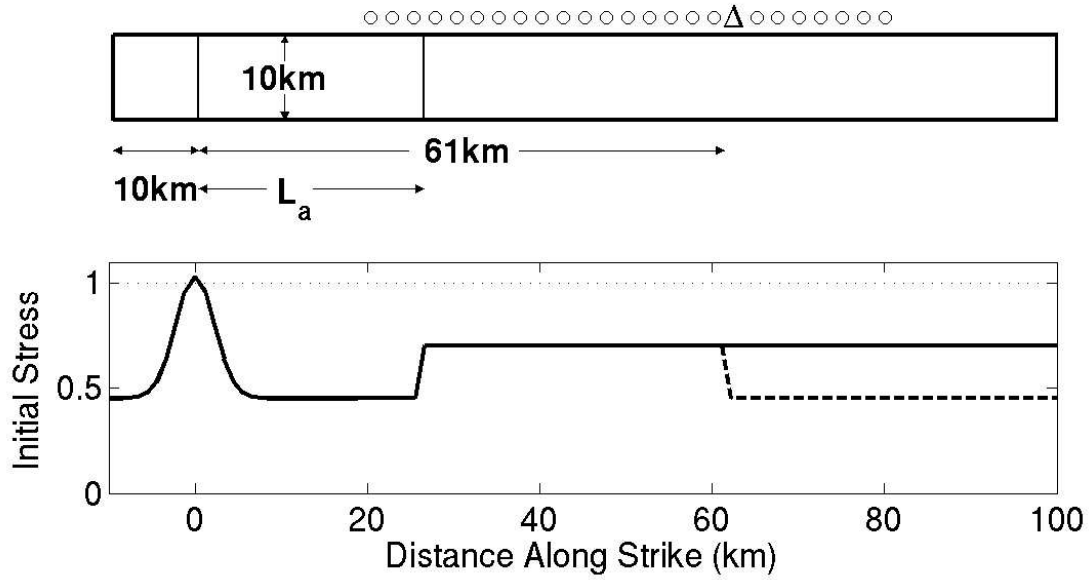


Figure 6: Model fault geometry and initial stress conditions (the solid line corresponds to model I; see table 1 for the parameters of the other models) used in the spontaneous rupture calculations. PS10 is marked with a triangle. Hypothetical stations spaced every 2.5 km between 20 km and 80 km, where we also compute ground motions, are denoted by small circles.  $L_a$  denotes the distance to the asperity, approximately 30 km. The initial stress profile marked by the dashed line shows the minimum width of the asperity required by the record of PS10, as discussed at the end of the text.

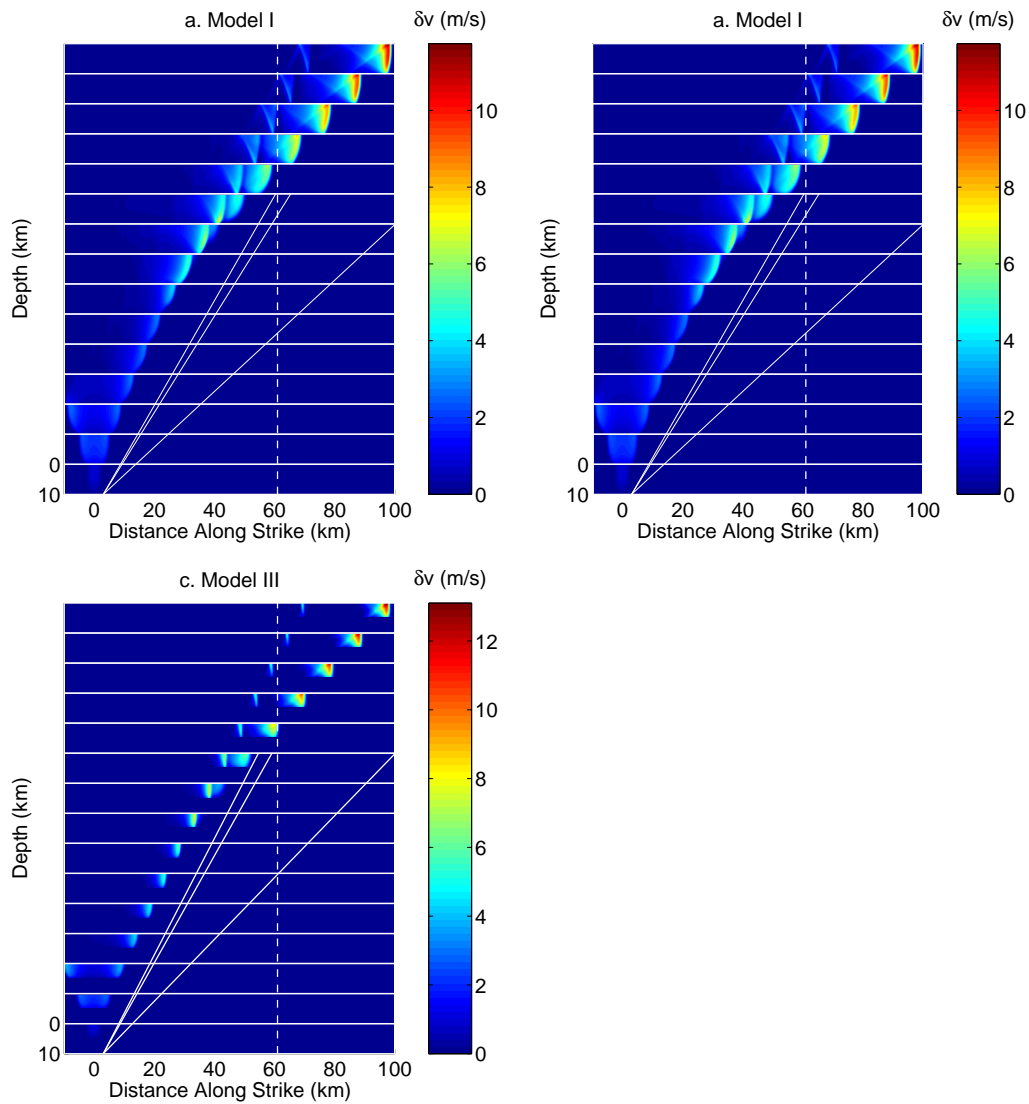


Figure 7: Snapshots of the fault surface with the color scale measuring slip velocity for (a.) model I (no healing, slip to 10 km depth, shown every 1.83 s), (b.) model II (including healing, slip to 10 km depth, shown every 1.83 s), and (c.) model III (no healing, slip to 5 km depth, shown every 1.65 s). Time advances from bottom to top. The solid white lines show wave speeds (Rayleigh, S, and P from bottom to top). The dashed white line marks the position of the station.

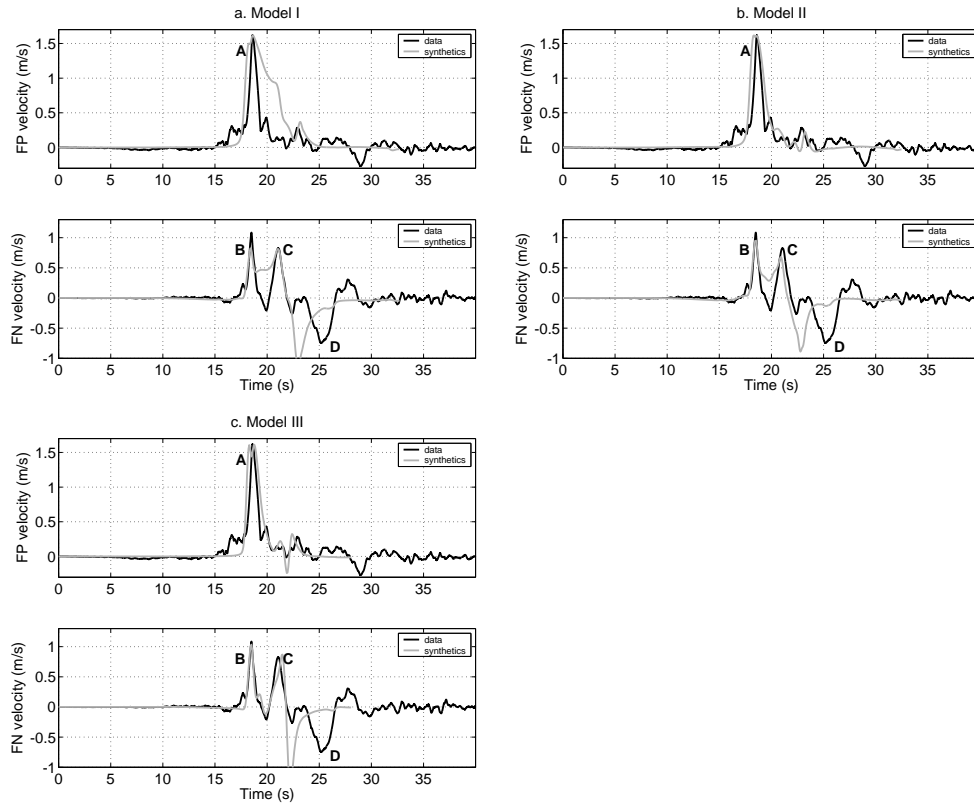


Figure 8: Comparison between recorded and synthetic ground motions at PS10 for (a.) model I (no healing, slip to 10 km depth), (b.) model II (including healing, slip to 10 km depth), and (c.) model III (no healing, slip to 5 km depth).

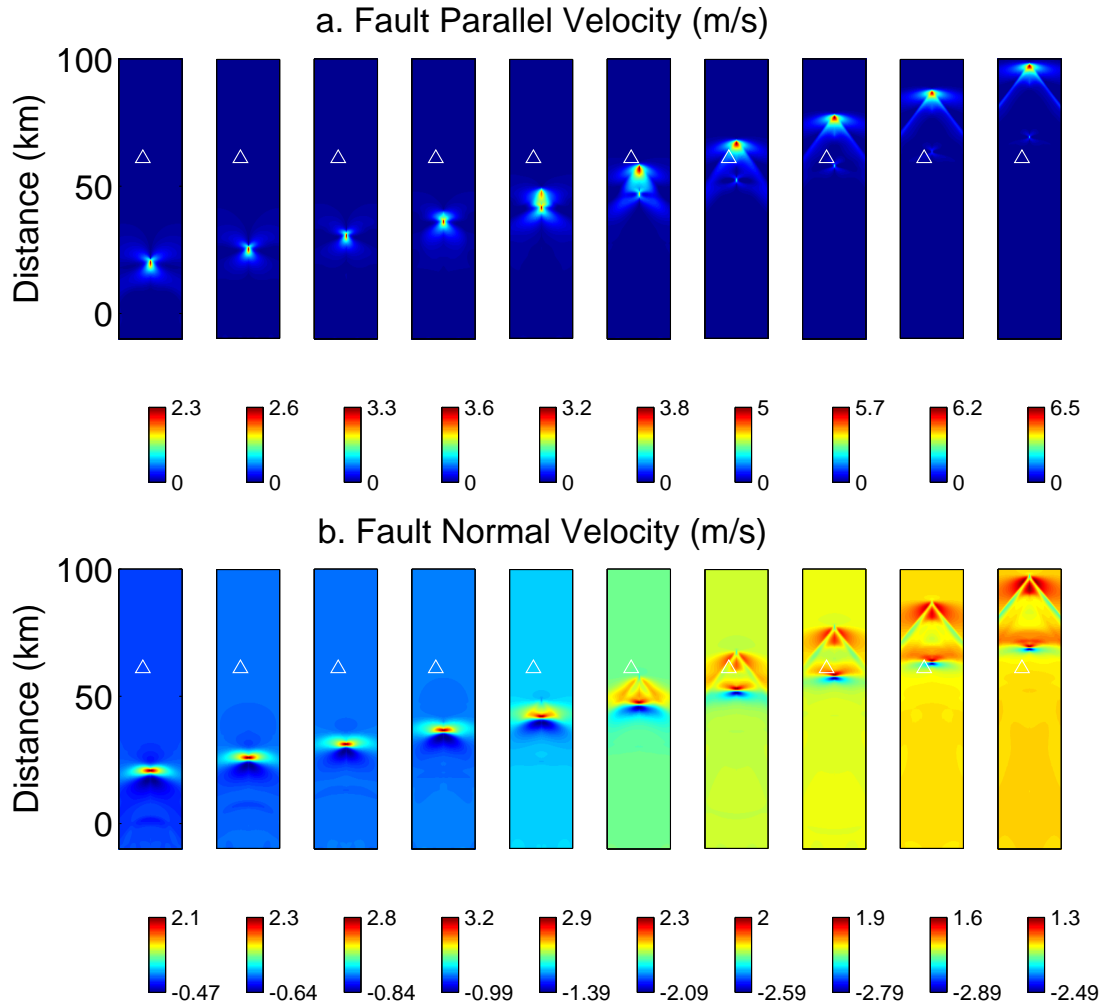


Figure 9: Snapshots of of the free surface showing (a.) fault parallel and (b.) fault normal ground motion every 1.28 s from left to right for model III, on an area extending 12.5 km to either side of the fault. Other models produce similar ground motion. The color scale, which changes for each snapshot, measures FP or FN velocity. Although the FP motion is antisymmetric across the fault, it is plotted as symmetric for visualization purposes. The location of PS10 is marked by the white triangle.

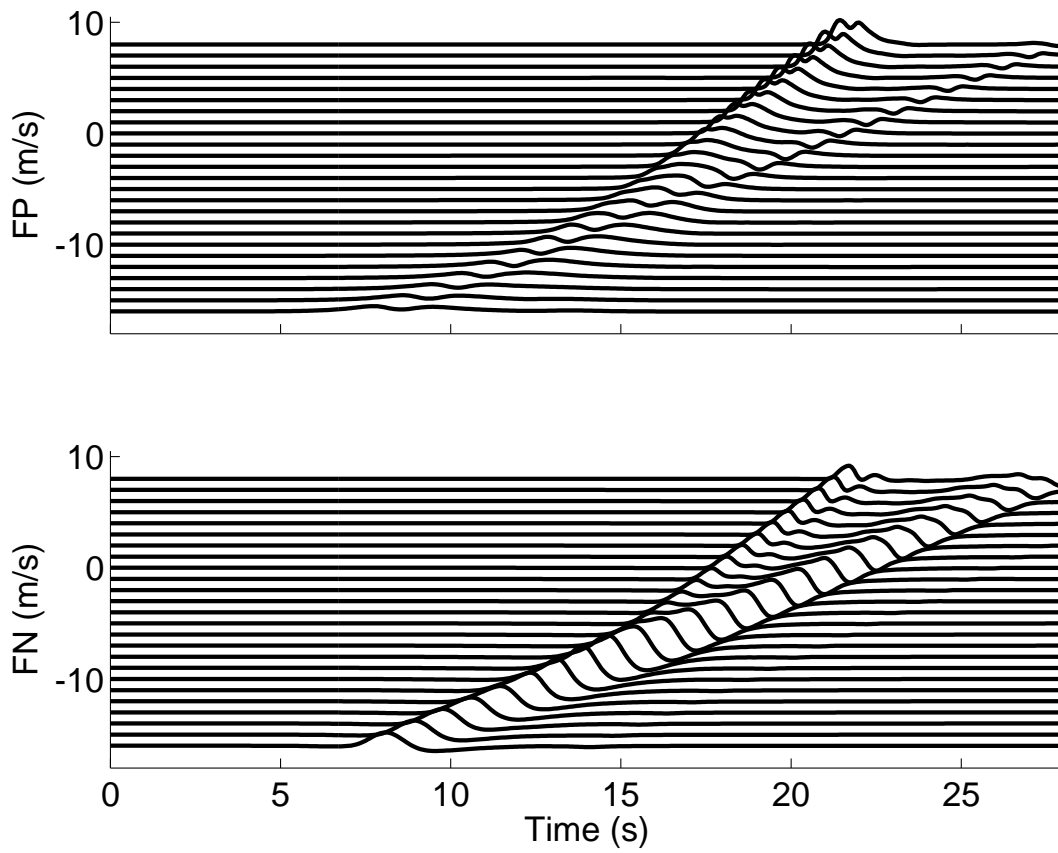


Figure 10: Particle velocities for model III recorded at a number of hypothetical stations every 2.5 km from 20 km to 80 km along a line parallel to and 3 km off the Denali fault, as shown in Figure 6. Adjacent traces are offset by 1 m/s with the record corresponding to the station at 60 km centered about zero.

Department of Physics  
University of California  
Santa Barbara, CA 93106  
(E.M.D.)

Department of Geological Sciences and Institute for Crustal Studies  
University of California  
Santa Barbara, CA 93106  
(R.J.A.)